Biomaterials 301 (2023) 122243

Contents lists available at ScienceDirect

Biomaterials

journal homepage: www.elsevier.com/locate/biomaterials

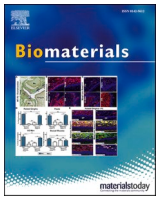

Understanding structure activity relationships of Good HEPES lipids for lipid nanoparticle mRNA vaccine applications

Rebecca L. Goldman [a], Namratha Turuvekere Vittala Murthy [c], Trent P. Northen [a], Anuranjani Balakrishnan [a], Sudha Chivukula [a], Hillary Danz [a], Timothy Tibbitts [a], Anusha Dias [a], Jorel Vargas [a], Dustin Cooper [a], Hardip Gopani [b], Angela Beaulieu [b], Kirill V. Kalnin [c], Timothy Plitnik [c], Saswata Karmakar [a], Ramesh Dasari [a], Ryan Landis [c], Shrirang Karve [a,*,1], Frank DeRosa [a]

[a] mRNA Center of Excellence, Sanofi, Waltham, MA, USA
[b] Translate Bio, Lexington, MA, USA
[c] Former Employee of Sanofi, Waltham, MA, USA

ARTICLE INFO

Keywords:
Lipid nanoparticle
mRNA vaccines
Liposomes
Ionizable lipid
Drug delivery
Cationic lipid
Structure activity

ABSTRACT

Lipid nanoparticles (LNPs) have shown great promise as delivery vehicles to transport messenger ribonucleic acid (mRNA) into cells and act as vaccines for infectious diseases including COVID-19 and influenza. The ionizable lipid incorporated within the LNP is known to be one of the main driving factors for potency and tolerability. Herein, we describe a novel family of ionizable lipids synthesized with a piperazine core derived from the HEPES Good buffer. These ionizable lipids have unique asymmetric tails and two dissimilar degradable moieties incorporated within the structure. Lipids tails of varying lengths, degrees of unsaturation, branching, and the inclusion of additional ester moieties were evaluated for protein expression. We observed several key lipid structure activity relationships that correlated with improved protein production *in vivo*, including lipid tails of 12 carbons on the ester side and the effect of carbon spacing on the disulfide arm of the lipids. Differences in LNP physical characteristics were observed for lipids containing an extra ester moiety. The LNP structure and lipid bilayer packing, visualized through Cryo-TEM, affected the amount of protein produced *in vivo*. In non-human primates, the Good HEPES LNPs formulated with an mRNA encoding an influenza hemagglutinin (HA) antigen successfully generated functional HA inhibition (HAI) antibody titers comparable to the industry standards MC3 and SM-102 LNPs, demonstrating their promise as a potential vaccine.

1. Introduction

In the last few years, the mRNA lipid nanoparticle (LNP) field has expanded dramatically and has become a household topic due to the COVID-19 pandemic. The success of the COVID-19 mRNA vaccines from Moderna, Pfizer/BioNTech, and others highlights the rapid manufacturing, efficacy, and tolerability that mRNA technologies have to offer [1–5]. mRNA-LNPs have potential for not only vaccine applications but also protein replacement therapies, personalized cancer vaccines, gene editing, and many other uses [6–10]. With this broad versatility, mRNA-LNPs as delivery vehicles offer a promising future of novel medical advancement.

The main driving factor for mRNA uptake and delivery into cells is the lipid nanoparticles which encapsulate the mRNA and protect it from the physiological environment [11]. LNPs are typically comprised of an ionizable/cationic lipid, pegylated lipid, cholesterol, and a

Abbreviations: LNP, lipid nanoparticle; HAI, hemagglutination inhibition; SAR, Structure Activity Relationship; HEPES, 4- (2- hydroxy ethyl)-1- piperazine ethane sulphonic acid; NHP, non-human primates; HA, hemagglutinin; mRNA, messenger ribonucleic acid; hEPO, human erythropoietin; IM, intramuscular; PEG, polyethylene glycol; PDI, polydispersity index; GP, generalized polarization; Cryo-TEM, cryogenic transmission electron microscopy; ELISA, enzyme-linked immunosorbent assay; SAR, structure activity relationship.

* Corresponding author.
E-mail address: Shri.Karve@sanofi.com (S. Karve).
[1] Author Address. mRNA Center of Excellence, Sanofi 200 West Street, Waltham, MA 02451.

https://doi.org/10.1016/j.biomaterials.2023.122243
Received 25 April 2023; Received in revised form 5 July 2023; Accepted 7 July 2023
Available online 8 July 2023

phospholipid. Selection of the ionizable or cationic lipid used within the LNP has been shown to influence the amount of mRNA delivery by mediating cell uptake and endosomal escape [12–14]. Many academic labs and companies have spent countless years and resources developing novel ionizable lipids and optimizing lipid structures to improve RNA delivery [12,15–22].

Ionizable lipids are amphiphilic with the hydrophilic part consisting of at least one tertiary amine that can become protonated under acidic conditions and a hydrophobic part with carbon tails of various length, with or without double bonds and degradable moieties. When formulated into an LNP, an ideal ionizable lipid allows for efficient cellular uptake aiding in adequate protein production *in vivo*, exhibit low toxicity, and demonstrate an acceptable clearance rate after injection [23–25]. Examples of widely used or well-known ionizable lipids include, DLin-MC3-DMA (MC3), ALC-315, SM-102, C12-200, cKK-E12, and OF-02 [22,25–31]. Several of these lipids have degradable moieties incorporated within the lipid structure, such as esters, that may potentially improve clearance of the lipid once administered into the body. Esters are the most incorporated degradable moiety and few alternatives have been investigated such as disulfides and amides [12,16,26,32,33]. Another feature infrequently mentioned in literature is the effect asymmetric lipid tails have on potency. This is because asymmetric lipid tails can be challenging to produce due to limitations in both chemical synthesis and commercially available reagents.

Herein, we describe a novel ionizable lipid family with a piperazine core derived from the Good buffers discovered by Norman Good in 1966 [34]. Specifically, we used the Good HEPES buffer as a base structure to synthesize over 250 chemically unique ionizable lipids containing different degradable moieties and carbon tails. The HEPES core structure with a hydroxyl and sulfonic acid group on either side allows for the ionizable lipid to contain an ester and disulfide degradable moieties, as well as asymmetric lipid tails on either arm of the final molecule (Fig. 1).

Two different lipid tail families, Generation 1 (Gen1) and Generation 2 (Gen2), were incorporated onto the Good HEPES core structure, with Gen2 structures focused on higher degradability. The Good lipids, in the form of LNPs, were screened *in vivo* with human erythropoietin (hEPO) mRNA, as a proof of concept, to test the delivery in mice after a single intramuscular (IM) injection. We observed several key lipid structure activity relationships (SARs) that correlated with improved protein production *in vivo*. Certain physical characteristics of the LNPs including structure and lipid bilayer packing were also shown to affect protein production. Additionally, Good lipid LNPs with HA successfully produced protein in a higher order animal model using non-human primates (NHPs) and generated functional neutralizing antibody titers against the influenza virus hemagglutinin 1 protein (HA1) when formulated with an mRNA encoding for an HA antigen.

2. Materials & methods

2.1. mRNA synthesis and lipid nanoparticle formulation

mRNA transcripts encoding for human EPO (hEPO) and hemagglutinin (HA) from A/California/04/2009 were synthesized by in vitro transcription employing RNA polymerase and unmodified nucleotides to transcribe the mRNA from a plasmid DNA template encoding the desired gene. The resulting purified precursor mRNA was reacted further *via* enzymatic addition of a 5′ cap structure (Cap 1) and an approximate 200 nucleotide 3′ poly(A) tail. Preparation of mRNA/lipid nanoparticle (LNP) formulations was described previously [35]. Briefly, an ethanolic solution of a mixture of lipids (ionizable lipid, dioleoylphosphatidylethanolamine, cholesterol, and polyethylene glycol-lipid) at a fixed lipid to mRNA ratio were combined with an aqueous buffered solution of target mRNA at an acidic pH under controlled conditions to yield a suspension of uniform LNPs. After ultrafiltration and diafiltration into a suitable diluent system, the resulting

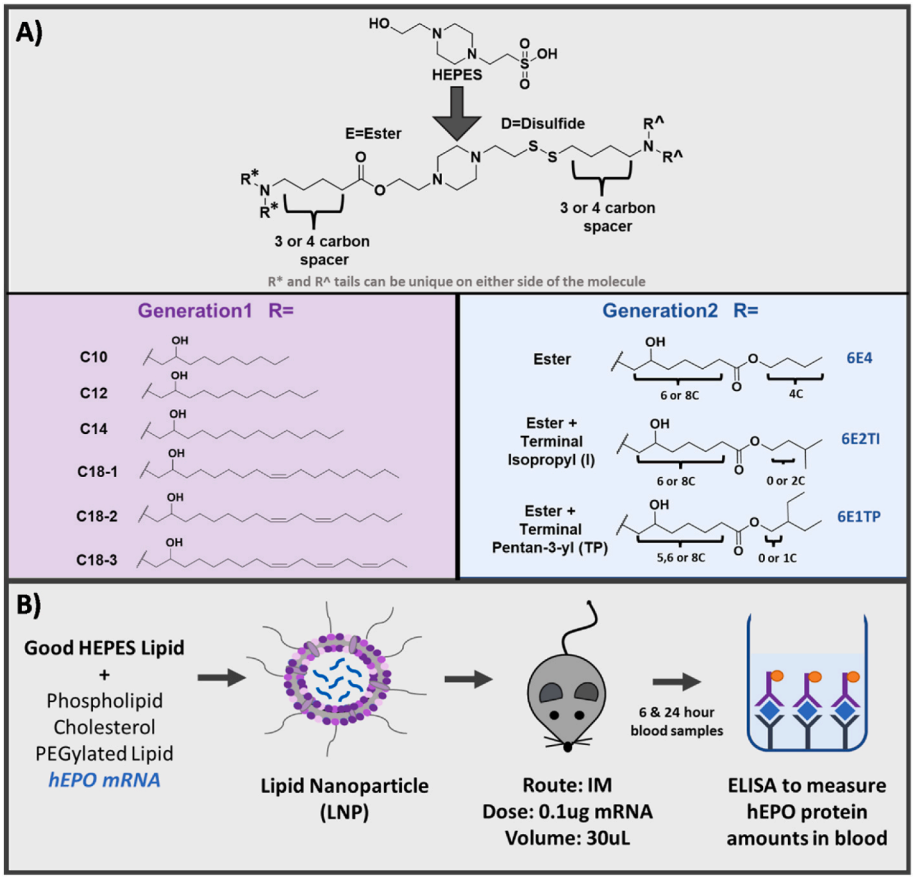

Fig. 1. Over 250 Good HEPES lipids were synthesized and screened for protein production in mice after a single IM injection. (A) Lipids were synthesized using the HEPES Good buffer as a core. One arm of the lipid contained a degradable disulfide bond and the other an ester. Spacer lengths of 3 or 4 carbons were incorporated in between the degradable bond and the tertiary amine. **The Generation 1 lipids** contained carbon tails that are 10, 12, 14, 18–1, 18–2, or 18–3 carbons in length. **The Generation 2** lipids contained 3 different carbon tails with additional esters and terminal carbon branches. The additional esters were spaced 5,6, or 8 carbons after the tertiary amine and the end of the lipid tail was either linear, contained a terminal isopropyl group (TI), or a terminal pentan-3-yl (TP). **(B)** The Good lipid nanoparticles were formulated with a PEG lipid, cholesterol, phospholipid and human EPO (hEPO) mRNA. The lipid nanoparticles were injected through intramuscular delivery to mice at a dose of 0.1 μg in 30 μL volume. hEPO levels were detected in the blood of the mice 6 and 24 h post injection with an ELISA assay.

nanoparticle suspensions were diluted to final concentration, filtered, and stored frozen at −80 °C until use. The molar composition used for lipid screening was as follows: 1.5:40:28.5:30 of polyethylene glycol-lipid: ionizable lipid: cholesterol: dioleoylphosphatidylethanolamine.

2.2. LNP characterization

mRNA encapsulation and concentration were measured using *RiboGreen*^{TM} assay using Quant-it Ribogreen Assay Kit (Thermo Fischer Scientific) according to the manufacture's protocol. Dynamic light scattering (DLS) was used to characterize LNP Z-average size, polydispersity (PDI), and zeta potential using a Malvern Zetasizer. Surface pKa of the LNPs was measured using the TNS (2-(p-toluidinyl)naphthalene-6-sulphonic acid) assay [36]. Briefly, LNPs were diluted into specific pH buffers ranging from pH 3–9 in increments of 0.5 and mixed with the TNS dye with a final concentration of 6 μM in each well. Fluorescence intensity was measured at excitation 322 nm and emission 431 nm. The LNP surface pKa was the pH at which 50% of the amine protonation occurred based off the fluorescence pH titration curves generated per LNP.

2.3. Laurdan assay

Formulations were diluted into buffer solutions at pH 4.5, 5.5, 6.5, or 7.5 and the laurdan molecule was added to a final laurdan concentration of 1 μM. Solutions were incubated at room temperature, protected from light, for 3 h. Samples were analyzed using a SpectraMax M5 Multi-Mode microplate reader. A fluorescence excitation wavelength of 340 nm was used along with emission wavelengths of 440 and 490 nm. GP values were calculated using the following equation: $GP = (AUC_{440} - AUC_{490})/(AUC_{440} + AUC_{490})$ [37,38].

2.4. Cryo-TEM imaging of the lipid nanoparticles

Samples were vitrified by plunge-freezing and imaged by brightfield cryo-transmission electron microscopy. TEM grids (Quantifoil GmbH) were glow-discharged for 25 s in rarefied room air using a Pelco EasiGlow (Ted Pella). Samples were applied to grids in the chamber of a Vitrobot Mk IV (ThermoFisher) at 95% relative humidity and 22 °C, blotted, and plunged into liquid ethane for vitrification. Each sample was vitrified on Quantifoil R2/1200 mesh grids both with and without a continuous carbon film of 2 nm nominal thickness. Imaging was performed on a Talos Arctica transmission electron microscope (FEI Company) with K2 direct electron detector (Gatan) controlled by SerialEM software [39] at 49,000 × and 130,000 × nominal magnification. Grids with and without continuous carbon were screened for each specimen and images were collected from grid showing optimal ice thickness and less contamination.

2.5. Animal studies

Ethics statement: Animal studies were conducted in compliance with all pertinent US National Institutes of Health regulations as well as with all relevant local, state, and federal regulations. Animal protocols were approved by the Institutional Animal Care and Use Committees (IACUCs) of the facilities at Alpha Preclinical (North Grafton, MA), Bioqual (Rockville, MD), and New Iberia Research Center (New Iberia, LA).

2.6. Mouse studies

Lipid screening studies were conducted with female BALB/cJ mice 6–8 weeks of age. Mice were dosed with 0.1 μg mRNA in 30 μL of LNPs by a single intramuscular (IM) injection into the gastrocnemius leg muscle. Blood samples were taken 6 and 24 h post injection and hEPO levels were measured in the blood serum of the mice using an ELISA assay according to the manufacture's protocol.

2.7. Non-human primate studies

Cynomolgus macaques of Mauritian origin 2–6 years of age and weighing in a range of 2–6 kg were administered 500 μL volume of formulations at a dose of 10 μg mRNA *via* intramuscular (IM) injection into the deltoid of the right forelimb on Day 0 and the left forelimb on Day 28. All immunizations and blood draws occurred under sedation with Ketamine HCl (10 mg/kg) or Telazol (4–8 mg/kg IM) [40].

2.8. Hemagglutinin inhibition (HAI) assay

HAI assays were performed as previously described [7] using the A/California/07/2009 (H1N1) virus stocks from BIOQUAL, Inc. Sera were treated with receptor-destroying enzyme (RDE) by diluting one-part serum with three parts enzyme and incubated overnight in a 37 °C water bath. Enzyme was inactivated by a 30-min incubation period at 56 °C followed by addition of six parts PBS for a final dilution of 1/10. HAI assays were performed in V-bottom 96-well plates using four hemagglutinating units (HAU) of virus and 0.5% turkey red blood cells. Reference serum was included as a positive control on every assay plate. Each plate also included a back-titration to confirm the antigen dose (4 HAU/25 μL) as well as a negative control sample (PBS or naive control serum). The HAI titer was determined as the highest dilution of serum resulting in complete inhibition of hemagglutination. Results were only valid for plates with the appropriate back-titration result (verifying 4 HAU/25 μL added) and a reference serum titer within 2-fold of the expected titer.

2.9. Statistical analysis

All statistics were calculated using the rstatix package in R (v 4.2.0). Significance was calculated using a Welch's *t*-test and p-values were adjusted for multiple hypothesis using the Bonferroni correction. The statistics for the HAI Fig. 6 were calculated using ANOVA and multiple comparisons were tested using Tukey honestly significant difference.

3. Results & discussion

3.1. A lipid library was synthesized derived from the good HEPES buffer

Over 250 lipids were synthesized using the HEPES core as shown in Fig. 1A. The HEPES buffer is cost-effective and widely used for cell culture applications, making the molecule a suitable candidate for synthesizing a large library of lipids [34]. The resulting ionizable lipids contained a piperazine core and asymmetric degradable bonds (ester on one side and disulfide on the other) (Fig. 1A) [34,41]. Each lipid contained two tails on each side of the HEPES core after the ester or disulfide for a total of four tails per lipid. The tails on the same side of the HEPES core were identical but could differ from the tails on the other side of the core. A spacer of three or four carbons was incorporated on either side of the molecule between the degradable bonds and tertiary amines. Each tertiary amine was connected to one of nine lipid tail structures. The Gen1 lipid tails consisted of carbon chains of 10, 12, 14, 18–1 (one double bond), 18–2 (two double bonds), or 18–3 (three double bonds) while Gen2 lipid tails contained an additional ester and different carbon spacer lengths before and after this added ester moiety (Fig. 1A). Isopropyl and pentan-3-yl terminal tail branches were also included in the Gen2 tails. A general synthesis pathway, representative NMR spectra and LC/MS of the Good lipids is provided in Fig. S1 &2.

Many Good lipids produced high amounts of hEPO protein after a single IM injection in mice. The Good HEPES lipids were formulated with hEPO mRNA to investigate lipid potency in mice upon a single IM administration. hEPO mRNA has been commonly used as a model protein for assessing LNP potency as it is an efficient and readily quantifiable method in mice [12,14,42–44]. To achieve effective mRNA delivery, Good HEPES lipids were formulated into LNPs by mixing a

Good ionizable lipid, a phospholipid, cholesterol, and a PEGylated lipid solution with an aqueous acidification buffer containing hEPO mRNA under controlled conditions. After ultrafiltration/diafiltration processing of the LNPs, mice were dosed with a single intramuscular (IM) injection of 0.1 μg LNPs based on mRNA concentration and blood samples were taken 6 and 24 h post-administration (Fig. 1B). An ELISA was performed to measure the amount of hEPO protein in the mouse blood serum at the aforementioned time points. For most Good lipid formulations, the average hEPO expression at 6 h was higher than 24 h, although in many cases these values were not significantly different (Fig. S3A). Numerous Gen1 Good lipids produced comparable if not higher amounts of hEPO protein compared to industry standard lipids, SM-102 and MC3. In general, we observed that Gen1 LNPs had significantly increased hEPO production compared to Gen2 lipids in mice (Fig. S3B). This may be attributed to the additional esters incorporated into the Gen2 tails, which may make the lipids more susceptible to degradation once administered *in vivo*. It is also worth noting that biodistribution studies revealed that with the low IM dose of 0.1 μg mRNA in LNPs, we only observed protein expression in the muscle tissue of the mice and not in other organs (Fig. S4).

The 6-h hEPO protein data was plotted as a heat map to better view lipid SARs for the Gen1 and Gen2 lipids (Fig. 2A and B). Darker colored squares on the heat map represent higher amounts of hEPO produced in mice 6 h after a single IM administration of 0.1 μg of mRNA. The Good lipid ester arm and tails are exemplified in the heat map columns while the disulfide lipid arm and tails are represented in the rows. An initial visual trend for Gen1 lipids on the ester side indicates that lipid tail lengths of 12 carbons produced more hEPO compared to other lengths and this trend was confirmed to be significant (Figs. 2B & 3A). In addition, lipid tail lengths of 18–3 (three double bonds) performed poorly, regardless of the lipid arm (Figs. 2B and 3A &B). This could be a result of the lower mRNA encapsulation of 18–3 LNPs, leading to inefficient mRNA delivery into the cells (Fig. S5E&F). Out of the 114 Gen2 lipids tested, 42 did not produce any detectable amount of hEPO and two lipids resulted in unstable formulations (UF) that were not dosed (Fig. 2B). Interestingly, almost all the high-performing lipids from Gen2 group were derived from lipid tails containing a terminal pentan-3-yl (TP) on either the ester or disulfide side of the molecule.

Further SAR analyses were performed to uncover structural aspects which affect LNP hEPO protein production *in vivo*. Viewing Fig. 3A, we confirmed that lipid tail length on the ester and disulfide side of the Good lipids played a significant role in influencing potency in both Gen1 and Gen2 LNPs. Gen2 lipid tails that contained an 8E1 terminal pentan-3-yl (8E1TP) moiety performed significantly better than the 6ETI tail on the ester side and the 6E4, 6ETI, and 6E2TI tails on the disulfide side (Fig. 3A and B). The biophysical characteristics of the 8E1TP LNPs were comparable to the other Gen2 tails and further experiments need to be performed to ascertain the reason why the 8E1TP tails benefited potency (Figs. S5A–F).

Another lipid structure aspect analyzed was the effect of the carbon spacer located between the tertiary amines and degradable ester or disulfide bond. Lipids containing either a 3 or 4 carbon spacer were synthesized and tested for hEPO production in mice (Fig. 3C). No potency difference related to the ester side was observed; however, lipids with a carbon spacer of 4 on the disulfide side resulted in significantly higher hEPO production in mice compared to a 3-carbon spacer in Gen1 lipids. This increase in protein production was surprising considering LNP encapsulation of Gen1 lipids was significantly lower for carbon spacers of 4 compared to 3 on the ester and disulfide lipid arms (Fig. S6C). Theoretically, small differences in carbon spacing may have affected LNP packing in a way that improved LNP potency. A weak correlation between lipid molecular weight and hEPO production *in vivo* was observed as well: Gen1 lipids with a lower molecular weight had greater potency, while the opposite trend was seen for Gen2 lipids (Fig. 3D). For additional viewing of lipid structure-activity trends, a table of each lipid tested, amount of hEPO produced, and the structure features are provided in Fig. S7.

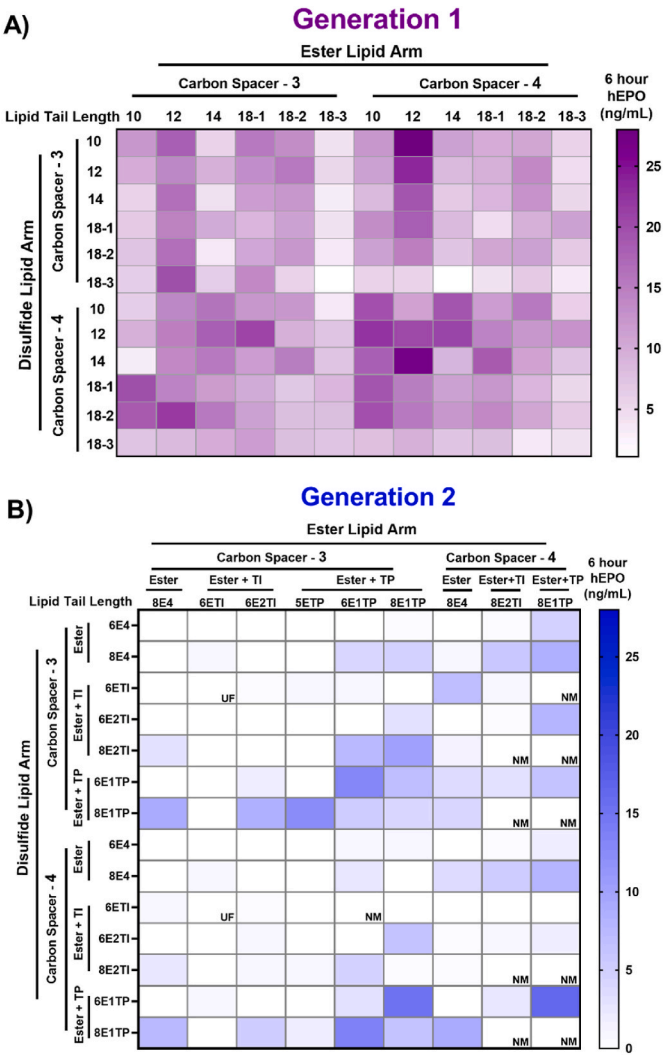

Fig. 2. Many of the Gen1 and Gen2 lipids produced high amounts of hEPO protein after a single IM injection in mice. The Good HEPES lipids were formulated for a single 30 μl IM injection of 0.1 μg in mice (n = 4). **(A) Many of the 144 Gen1 lipids produced high amounts of hEPO in mice and revealed lipid structure and potency trends**. Heat map of the average 6-h timepoint where the darker color indicates a higher hEPO protein amount. Visually, lipids with carbon tails of 12 on the ester arm of the lipid performed better while 18–3 tails performed worse. **(B) The Gen2 lipids were overall less potent compared to Gen1**. Several tail structures including the additional Ester + Terminal Pentan-3-yl (TP) improved the hEPO production in mice for the Gen2 lipids. Each square on the heat maps represents the average hEPO protein value produced in n = 4 mice. **UF** = unstable formulation. **NM** = lipid never made.

3.2. LNP biophysical characteristics and relationship with potency

Next, the formulation potency was assessed in relation to biophysical properties of LNPs, such as LNP size, mRNA encapsulation, surface pK_a, and zeta potential (Fig. 4). A size range of ~60 nm–~150 nm was observed for both Gen1 and Gen2 LNPs (Fig. 4A). The formulations with superior performance had diameters around 80 and 120 nm for the Gen1 and Gen2 LNPs, respectively, while no significant correlation between *in vivo* potency and size of LNPs was detected. However, it was observed that larger Gen1 LNPs were dependent on lipid tail structure where double bonds incorporated in the tails resulted in larger LNPs on the disulfide arm and specific Gen2 lipid tails resulted in larger LNP size compared to others (Fig. S5 A&B).

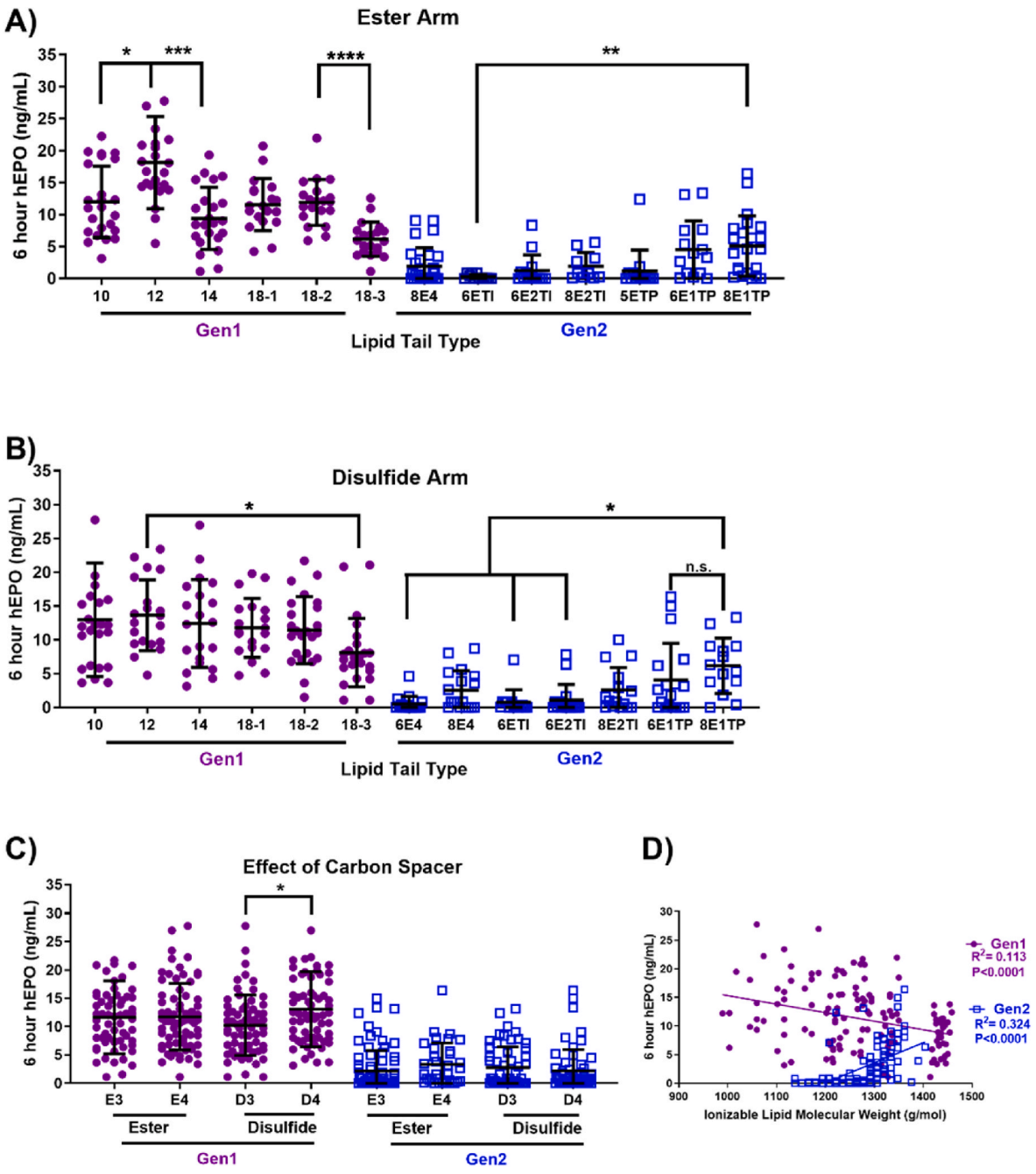

Fig. 3. Lipid tail type, carbon spacing, and lipid molecular weight significantly influenced amount of protein produced in mice. (A) For Gen1, lipids with carbon tail lengths of 12 on the ester arm produced significantly better hEPO and the 18–3 tails produced less. The Gen2 tails containing the 8E1TP groups performed better compared to the 6ETI Gen2 tails **(B)** Similarly to the ester arm, the 18–3 carbon tails performed significantly worse compared to other Gen1 tails tested for the disulfide arm of the Good lipids. The carbon tails with the 8E1TP group produced the highest amount of hEPO compared to several other Gen2 lipids. **(C)** A carbon spacer of 4 carbons on the disulfide arm of the lipid significantly improved hEPO protein expression compared to 3 carbons for the Gen1 lipids. There was no significant difference between carbon spacer lengths for the Gen2 lipids in relation to hEPO produced. **(D)** The molecular weight of the lipid had a weak correlation with amount of hEPO produced at 6 h in mice. For Gen1, lipids with lower molecular weight had higher hEPO expression and for Gen 2, lipids with higher molecular weight had higher hEPO expression. Each dot on the graphs represents the average hEPO protein amount of n = 4 mice. The black horizontal and vertical bars are the mean values for each population and the standard deviation, respectively. *p < 0.05, **p < 0.01, ***p < 0.001, ****p < 0.0001. Statistical significance was evaluated using a Welch's *t*-test.

The Polydispersity (PDI) trended higher for Gen2 LNPs compared to Gen1 suggesting that Gen1 LNPs have a more mono-dispersed particle population (Fig. S5C&D). Additionally, mRNA encapsulation did not correlate with *in vivo* potency in mice for the separate Gen1 and Gen2 families, although it was noted that Gen2 lipids had a greater number of LNPs with encapsulation efficiencies below 70% whereas most Gen1 lipids had encapsulation efficiencies of >80% (Fig. 4B and Fig. S5E&F).

Apparent pK_a of the LNPs was measured for 60 formulations using a TNS assay to assess particle protonation on the LNP surface. Gen1 LNPs had lower surface pK_a values ranging from 5.2 to 6.3 while Gen2 lipids values ranged from 5.8 to 6.9 (Fig. 4C). Interestingly, the best performing lipids *in vivo* from both Gen1 and Gen2 had similar pK_a values of 6.0 and 6.2. These pK_a values observed were comparable to published values such as that of the Acuitas ALC-0315 mRNA formulation with a

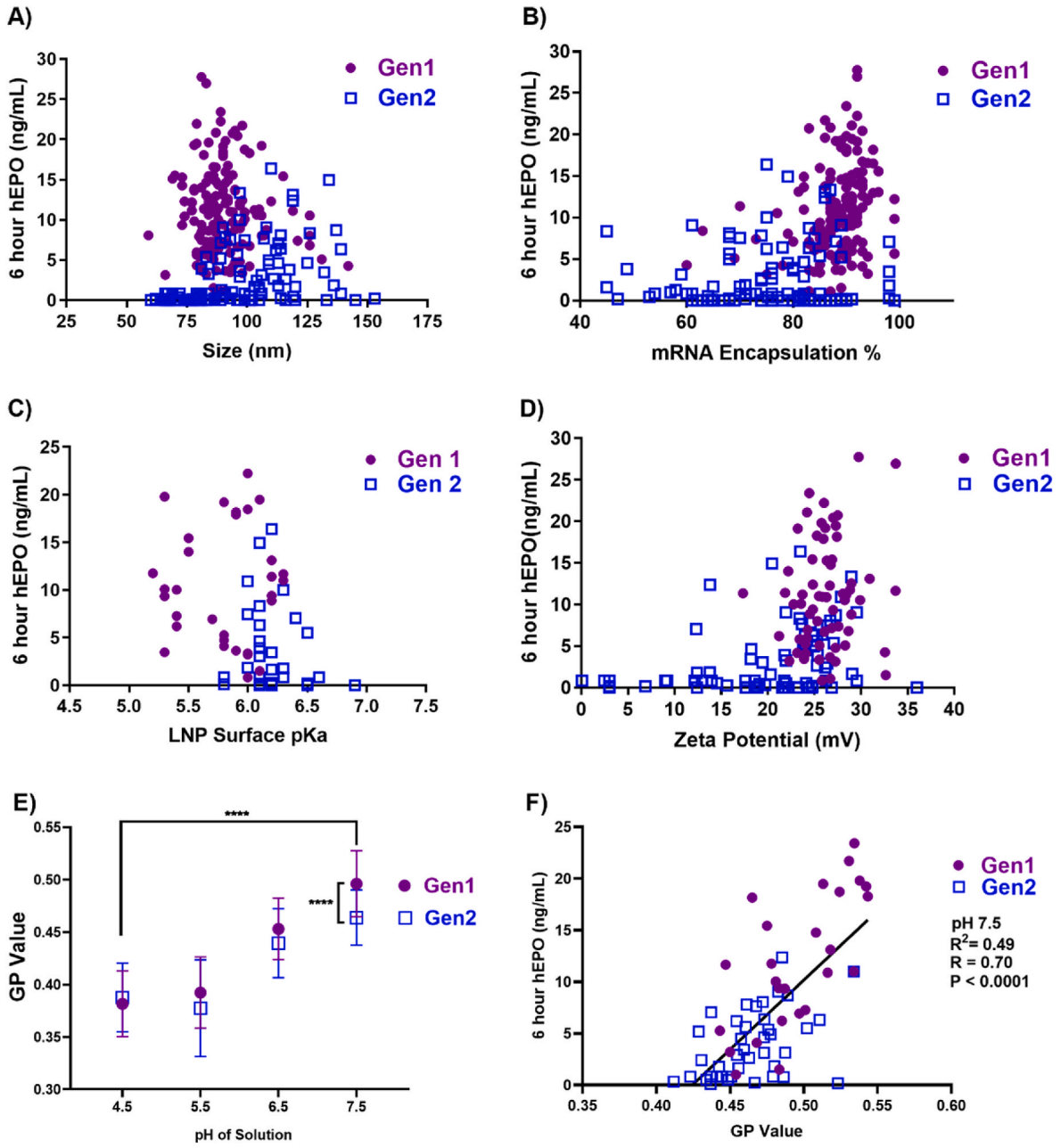

Fig. 4. LNP physiological characteristics and relationship with protein production for Gen1 and Gen2 lipids. The Good LNPs were characterized for diameter size, mRNA encapsulation%, LNP surface pKa, surface zeta potential, and lipid bilayer packing to investigate trends with amount of hEPO produced in mice. **(A) The Good LNPs ranged in size from 60–150 nm and no significant correlation was observed with potency.** The top performing formulations had a diameter of 80 and 120 nm for the Gen1 and Gen2 LNPs, respectively. Size was measured using dynamic light scattering. **(B) Overall, more of the Gen2 LNPs had lower mRNA encapsulation% compared to Gen1 and no significant correlation was observed with potency in mice.** mRNA encapsulation was measured with a Ribogreen™ assay according to the manufacturer's protocol. **(C) The surface pK_a of LNPs ranged from 5.2–6.9 and no correlation was seen between pK_a and hEPO produced in mice.** The Gen1 LNPs tended to have lower pKa values compared to Gen2. Surface pKa was measured using a TNS assay. **(D) Good LNPs with zeta potentials less than 12 mVs did not produce any protein in mice.** The Gen1 LNPs had a narrower range of Zeta potential compared to Gen2. Zeta potential was measured in 1 mM KCl. **(E) The laurdan generalized polarization (GP) value decreased in lower** pH **buffers of 5.5 and 4.5 for all formulations tested, and Gen1 had higher overall GP value at** pH **7.5.** Gen1 & Gen2 formulations were incubated with the laurdan probe under pH 4.5, 5.5, 6.5, and 7.5 buffer conditions. The GP value was calculated based off fluorescence values to give an idea of formulation lipid membrane packing. **(F) A positive linear correlation was found between the laurdan GP value and the amount of hEPO produced at 6 h in mice**. For Gen1 and Gen2, an increase in GP value correlated with an increase in hEPO protein in pH 7.5 solution. Each dot or square on the graphs represents the average hEPO protein amount of n = 4 mice.***$p < 0.001$ ****$p < 0.0001$ Statistical significance was evaluated using a Welch's *t*-test.

reported pKa of 6.09 [31]. Alabi et al. observed that siRNA LNPs with surface pK_as ranging from 6 to 7 had the best potency *in vivo* and Whitehead et al. observed a pK_a of 5.5 or higher is critical for *in vivo* transfection ability [16,33]. In addition, Hassett and Patel et al. have reported their top performing ionizable lipids for IM delivery have pK_as around 6.75 [28,31]. Variances in optimal LNP surface pK_a could be due to differences in lipid structure, helper lipid, and LNP composition. All these factors can affect the chemical structure presented on the LNP surface, the fraction of ionizable lipid that is protonated, and determine the final apparent pK_a.

All LNPs tested had a positive or neutral zeta potential and we did not detect a significant correlation with hEPO production in mice (Fig. 4D). It was observed that LNPs with zeta potentials below 12 mVs did not result in any hEPO protein production suggesting a higher positive surface charge is required for LNP efficacy. The lower zeta potential of Gen2 LNPs could be due to additional ester groups in the lipid tails causing alternative LNP packing and changing the structural entities presented on the surface and the overall LNP surface charge.

The LNP laurdan GP value at pH 7.5 correlates with hEPO production *in vivo*. We utilized the laurdan probe to better understand lipid packing for the Good LNPs. The laurdan probe inserts itself homogeneously into the hydrophilic/hydrophobic interface of the lipid bilayer and is used to measure polarity changes in the bilayer environment which can be related to lipid membrane packing and orderliness [45–47]. A generalized polarization (GP) value was calculated from a shift in fluorescence intensity of 440 nm–490 nm when the laurdan probe interacts with water molecules in the lipid membrane. A lower GP value is associated with a hydrated and fluid membrane while a higher GP value typically means less water molecules and more ordered lipid packing [37]. The GP value of Gen1 and Gen2 LNPs was measured in pH 7.5, 6.5, 5.5, and 4.5 buffers to simulate endosomal pH shift that occurs when particles are taken up by cells. It was observed that lower pH levels (4.5 and 5.5) resulted in lower GP values for all formulations tested compared to pH 6.5 and 7.5 (Fig. 4E). This suggests that LNPs are becoming more fluid and less orderly when the pH environment decreases, which is consistent with what Koitabashi et al. observed for the ionizable lipid DLin-KC2-DMA [37]. We also detected that Gen1 LNPs had overall higher GP value at pH 7.5 compared to Gen2 LNPs. The lower GP value of Gen2 at pH 7.5 may be due to the additional esters or potentially carbon branches in the lipid tails could have resulted in a more fluid bilayer compared to Gen1 lipid tails. Interestingly, a positive trend was observed between GP value and amount of hEPO produced in mice at pH 7.5 for Gen1 and Gen2 LNPs (Fig. 4F). The results suggest that GP value correlation with *in vivo* potency may be unique and specific to ionizable lipid family and pH tested. One hypothesis for the slight correlation between GP value at pH 7.5 and protein production is that particles with tighter bilayer packing may perform better *in vivo* by increasing LNP stability under physiological pH conditions. Further studies would need to be performed to increase understanding of how the GP value relates to desired LNP characteristics.

LNPs that produced different protein amounts had varied internal structures. From the current findings, Gen1 lipids demonstrated the ability to effectively deliver hEPO *in vivo* and had desirable LNP characteristics. For these reasons we decided to purse only Gen1 lipids for further evaluation. A selection of Good LNPs from the Gen1 lipids were imaged using Cryo-TEM to investigate potential correlations between particle internal structures and *in vivo* potency. Three LNPs were selected based on hEPO protein produced in mice: a low (Lipid 6), mid (Lipid 91), and high (Lipid 144) LNP were vitrified by plunge-freezing, imaged by brightfield Cryo-TEM and two representative images per LNP

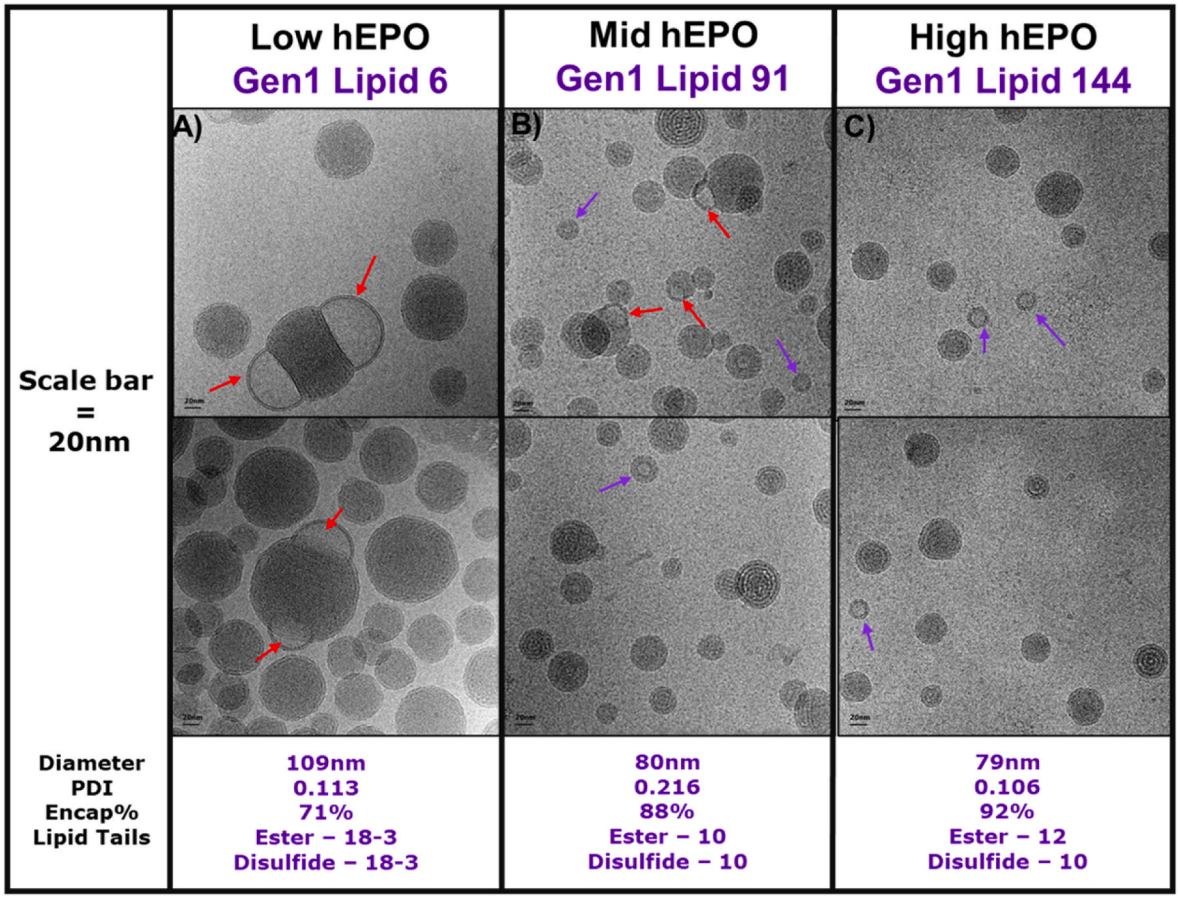

Fig. 5. Cryo-TEM images revealed changes in LNP structure for three formulations that produced different amounts of protein in mice. Three different Good LNPs were prepared for Cryo-TEM imaging that produced varying amounts of hEPO in mice. Blebs are shown with red arrows and particles with a smaller lipid bilayer and less dense core are seen with purple arrows. **(A) LNPs formulated with Lipid 6 from Gen1 were visually larger than the others and contained many blebs**. The Lipid 6 LNP internal structures looked relatively uniform and full of cargo with a lipid bilayer and solid core. **(B) LNPs formulated with Lipid 91 from Gen1 contained several blebs and some particles with a less-dense core.** Some of the structures looked multilamellar and others a lipid bilayer with solid core. **(C) The highest protein producing LNPs formulated with lipid 144 contained many small particles that had a single lipid bilayer and less dense core.** There were no blebs observed in the Good lipid 144 particles and many uniform multilamellar structures seen were seen. Scale bars in images are 20 nm.

were selected for the main body of this publication (Fig. 5). Additional images of the three Good lipids tested can be found in the supplementary data Fig. S8. Cryo-TEM images of Lipid 6 LNPs show these structures were notably larger in size compared to Lipids 91 and 144 and contained numerous bleb structures (red arrows) (Fig. 5A). The internal structure of Lipid 6 had a distinct outer lipid bilayer with either a solid core or non-multilamellar structure on the inside. Additionally, all Lipid 6 LNPs appeared dense in the core compared to the outside solution indicating they have either lipids or mRNA inside. Similar to Lipid 6 low-hEPO LNPs, Lipid 91 mid-hEPO LNPs showed many blebs throughout the images (Fig. 5B). An interesting observation was the appearance of nanoparticles that have a less-dense core, and could potentially be empty or have less cargo. The internal structure of potentially empty particles (purple arrows) had a similar density to the outside solution and were often smaller in size. High-hEPO producing Lipid 144 LNPs had similar characteristics as Lipid 91 with a mixture of multilamellar structures and the small less-dense core particles that may be empty (purple arrows Fig. 5C). Blebs were not observed in Lipid 144 LNPs leading us to hypothesize that bleb structures in Good LNPs may have a negative effect on potency. In contrast, the small, potentially empty particles may improve potency as they were abundant in mid and high hEPO producing LNPs.

The commonly reported internal structure for mRNA LNPs is the multilamellar structure or the single lipid bilayer with a solid core [42,47,48]. The bleb structure has been noted in several other formulations in literature including one of the currently approved mRNA lipid nanoparticle vaccines [49–51]. Leung et al. has also reported that bleb structures occurred in DLin-KC2-DMA mRNA formulations when the helper lipid DSPC was used but not with DOPE [52]. Additionally, Arteta et al. showed that MC3 mRNA formulations contained blebs, however, the authors only noticed them in the smaller particles [53]. Overall, changing any part of the formulation, ionizable lipid, helper lipid, composition, *etc*., is likely to result in a different particle internal structure making it very specific to what combination is evaluated [54].

Good LNPs produced protein in NHPs and generated neutralizing antibodies when formulated as an influenza mRNA vaccine. To validate the hEPO protein results observed in mice that were administered Good LNPs, we investigated protein production in a higher order animal model using the cynomolgus macaque non-human primate (NHP) model. NHPs received a single 10 μg dose of Gen1 LNPs formulated with hEPO mRNA by IM injection and sera was collected at 6, 24, 48, 72, and 96 h post-administration. All Gen1 Good LNPs tested produced quantifiable hEPO protein amounts in NHPs with an average peak occurring at 24 h for all LNPs except those formulated with Lipid 32 where the average peak occurred at 6 h (Fig. S9A). The Lipid 125 formulation resulted in the highest average amount of hEPO, although this was not significant due to biological variability. When comparing the average protein peaks in both animal models, the 6-h peak of expression in mice had a significant linear correlation with the 24-h peak in NHPs (Fig. S9B). To better understand how these lipids affected the animals, a number of physiological readouts were taken 3-days prior to administration (pre-study), 24-h, and 96-h post-administration (Figs. S9C–G). While fibrinogen (Fig. S9C) and AST (Fig. S9E) all showed declining levels at 96-h after an initial spike at 24-h post-administration, ALT levels did not decrease much at 96-h and for some lipids, even increased. However, most animals remained either within the upper limit of the normal range for ALT (≤85 U/L) or were within a 2.5-fold increase, which is considered mildly elevated (Fig. S9D). Two key cytokines were also evaluated at 24-h post-administration, IL-6 (Fig. S9F) and IFNγ (Fig. S9G) where a similar pattern was observed with Lipid #57 resulting in the highest induction of all three cytokines.

Next, we examined how the Gen1 Good LNPs would perform as potential influenza vaccines. Good lipids were formulated with mRNA encoding the hemagglutinin (HA) antigen from the A/California/04/2009H1N1 strain of influenza. Influenza-naïve NHPs were administered mRNA-LNPs at Day 0 and Day 28 by IM injection at a dose of 10 μg. Neutralizing antibody titers were determined by HAI (Fig. 6). All formulations tested induced neutralizing antibodies against the homologous virus strain in NHPs after two administrations (Day 42) and several formulations even had detectable titers after a single administration (Day 28). Of note, Good LNPs formulated with Lipids 28, 57, 109 and 122 induced HAI titers comparable to industry standard lipids MC3 and SM-102. Prior studies have indicated the ability of vaccines to produce neutralizing antibodies against the recombinant HA protein provides protection against the influenza virus [7,55,56]. Our study highlights the potential of Good lipids for development as mRNA-based vaccine candidates.

4. Conclusion

The novel family of Good lipids described here represent a promising vehicle for mRNA vaccine delivery. Key aspects of lipid structure that influence the level of target protein expression *in vivo* were identified. Specifically, modifications of lipid tail, carbon spacer, and lipid molecular weight played a major role in LNPs' biophysical characteristics and *in vivo* potency. Noticeably, the addition of esters into the tails for Gen2 lipids significantly reduced protein expression in mice. The lipid polarity/membrane packing measured with the laurdan probe may be a beneficial tool for rapid identification of promising ionizable lipids; however, further studies are required to verify this approach. In addition, a potential limitation for this body of work is one formulation composition was utilized for screening all Good lipids and there is a possibility the SAR understandings would be different if several compositions were attempted.

The internal LNP structure, visualized by Cryo-TEM, was useful to identify structural differences and speculate on their effects on formulation potency. In particular, the formulations that yielded superior

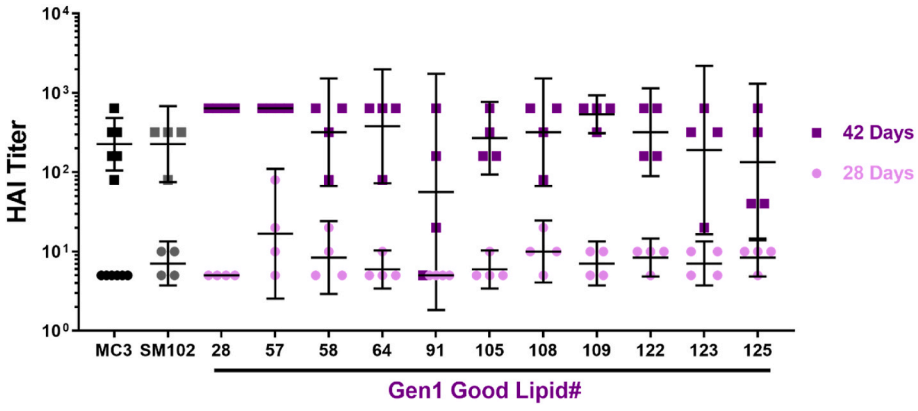

Fig. 6. Good lipids generated functional HAI antibody titers in non-human primates (NHPs) after administration of LNPs containing an influenza antigen mRNA. LNPs were formulated with mRNA that encodes for an influenza virus antigen and NHPs were immunized at day 0 and day 28 with a dose of 10 μg. Serum was collected at day 28 and day 42 to measure functional antibody titers by HAI. Several Gen1 Good Lipids produced similar HAI titers compared to MC3 and SM102 at day 42. (n = 4). Each dot or square on the graph represents individual NHP animal titer values. The black horizontal lines and error bars represent the geometric mean with 95% confidence intervals, respectively. The values within the timepoints were not significant from one another as determined by an ANOVA with multiple comparisons using Tukey HSD.

performance did not contain bleb structures, but they are distinguished by uniform multilamellar structures with smaller sized, less-dense core particles. The Good lipids successfully produced protein in NHPs and generated functional HAI antibody titers when formulated with an influenza HA mRNA. Several of the LNPs tested produced HAI titers comparable to the industry standard SM-102 and MC3 formulations. With this breadth of compelling data, we suggest that this novel lipid family holds great potential as a safe and effective means for delivery a wide range of mRNA vaccines.

Credit author statement

Rebecca L. Goldman: Conceptualization, Investigation, Writing – Original Draft, Writing – Review & Editing, Visualization. **Namratha Turuvekere Vittala Murthy**: Investigation, Visualization, Formal Analysis, Writing – Original Draft. **Trent P. Northen:** Investigation, Visualization, Formal Analysis, Writing – Original Draft. **Anuranjani Balakrishnan**: Investigation, Visualization, Formal Analysis. **Sudha Chivukula:** Investigation, Writing – Review & Editing. **Hillary Danz:** Writing – Original Draft, Writing – Review & Editing, Formal Analysis, Visualization. **Timothy Tibbitts:** Investigation. **Anusha Dias:** Investigation. **Jorel Vargas:** Investigation. **Dustin Cooper:** Investigation. **Hardip Gopani**: Investigation. **Angela Beaulieu:** Investigation. **Kirill V. Kalnin:** Investigation, Writing – Review & Editing. **Timothy Plitnik:** Investigation. **Saswata Karmakar:** Writing – Review & Editing, Investigation, Visualization. **Ramesh Dasari:** Writing – Review & Editing, Investigation, Visualization. **Ryan Landis:** Investigation. **Shrirang Karve**: Supervision, Conceptualization, Writing – Review & Editing. **Frank DeRosa:** Supervision, Conceptualization, Writing – Review & Editing.

Author contributions

The manuscript was written through contributions of all authors. All authors have given approval to the final version of the manuscript.

Funding sources

The research included in the manuscript was funded by Sanofi.

Declaration of competing interest

The authors declare the following financial interests/personal relationships which may be considered as potential competing interests: Frank DeRosa reports a relationship with Sanofi Pasteur that includes: employment and equity or stocks. Shrirang Karve reports a relationship with Sanofi Pasteur that includes: employment and equity or stocks. Rebecca Goldman reports a relationship with Sanofi Pasteur that includes: employment and equity or stocks. Anusha Dias reports a relationship with Sanofi Pasteur that includes: employment and equity or stocks. Jorel Vargas reports a relationship with Sanofi Pasteur that includes: employment and equity or stocks. Dustin Cooper reports a relationship with Sanofi Pasteur that includes: employment and equity or stocks. Kirill Kalnin reports a relationship with Sanofi Pasteur that includes: employment and equity or stocks. Tim Tibbitts reports a relationship with Sanofi Pasteur that includes: employment and equity or stocks. Sudha Chivukula reports a relationship with Sanofi Pasteur that includes: employment and equity or stocks. Saswata Karmakar reports a relationship with Sanofi Pasteur that includes: employment and equity or stocks. Ramesh Dasari reports a relationship with Sanofi Pasteur that includes: employment and equity or stocks. Shrirang Karve, Frank DeRosa, Ryan Landis, Ramesh Dasari, and Saswata Karmakar has patent “Good” Buffer-Based Cationic Lipids issued to Sanofi Pasteur.

Data availability

Data will be made available on request.

Acknowledgements

The authors would like to thank Jason Kaelber from the RCNF at Rutgers university for the Cryo-TEM images. We would also like to thank Emma McIntosh for statistical analysis and Natalia Vargas-Montoya for the LNP cartoon. The authors would like to thank Barak Yahalom at Alpha Preclinical for managing all *in-vivo* studies and for his contributions to the research presented in this manuscript.

Appendix A. Supplementary data

Supplementary data to this article can be found online at https://doi.org/10.1016/j.biomaterials.2023.122243.

References

[1] L.R. Baden, H.M.E. Sahly, B. Essink, K. Kotloff, S. Frey, R. Novak, D. Diemert, S. A. Spector, N. Rouphael, C.B. Creech, J. McGettigan, S. Khetan, N. Segall, J. Solis, A. Brosz, C. Fierro, H. Schwartz, K. Neuzil, L. Corey, P. Gilbert, H. Janes, D. Follmann, M. Marovich, J. Mascola, L. Polakowski, J. Ledgerwood, B.S. Graham, H. Bennett, R. Pajon, C. Knightly, B. Leav, W. Deng, H. Zhou, S. Han, M. Ivarsson, J. Miller, T. Zaks, C.S. Group, Efficacy and safety of the mRNA-1273 SARS-CoV-2 vaccine, N. Engl. J. Med. 384 (2020) 403–416, https://doi.org/10.1056/nejmoa2035389.

[2] P.B. Gilbert, D.C. Montefiori, A.B. McDermott, Y. Fong, D. Benkeser, W. Deng, H. Zhou, C.R. Houchens, K. Martins, L. Jayashankar, F. Castellino, B. Flach, B. C. Lin, S. O'Connell, C. McDanal, A. Eaton, M. Sarzotti-Kelsoe, Y. Lu, C. Yu, B. Borate, L.W.P. van der Laan, N.S. Hejazi, C. Huynh, J. Miller, H.M.E. Sahly, L. R. Baden, M. Baron, L.D.L. Cruz, C. Gay, S. Kalams, C.F. Kelley, M.P. Andrasik, J. G. Kublin, L. Corey, K.M. Neuzil, L.N. Carpp, R. Pajon, D. Follmann, R.O. Donis, R. A. Koup, Immune correlates analysis of the mRNA-1273 COVID-19 vaccine efficacy clinical trial, Science 375 (2021) 43–50, https://doi.org/10.1126/science.abm3425.

[3] N. Khehra, I. Padda, U. Jaferi, H. Atwal, S. Narain, M.S. Parmar, Tozinameran (BNT162b2) vaccine: the journey from preclinical research to clinical trials and authorization, AAPS PharmSciTech 22 (2021) 172, https://doi.org/10.1208/s12249-021-02058-y.

[4] S.J. Thomas, E.D. Moreira, N. Kitchin, J. Absalon, A. Gurtman, S. Lockhart, J. L. Perez, G.P. Marc, F.P. Polack, C. Zerbini, R. Bailey, K.A. Swanson, X. Xu, S. Roychoudhury, K. Koury, S. Bouguermouh, W.V. Kalina, D. Cooper, R.W. Frenck, L.L. Hammitt, Ö. Türeci, H. Nell, A. Schaefer, S. Ünal, Q. Yang, P. Liberator, D. B. Tresnan, S. Mather, P.R. Dormitzer, U. Şahin, W.C. Gruber, K.U. Jansen, C.C. T. Group, Safety and efficacy of the BNT162b2 mRNA covid-19 vaccine through 6 months, N. Engl. J. Med. 385 (2021) 1761–1773, https://doi.org/10.1056/nejmoa2110345.

[5] E.D. Moreira, N. Kitchin, X. Xu, S.S. Dychter, S. Lockhart, A. Gurtman, J.L. Perez, C. Zerbini, M.E. Dever, T.W. Jennings, D.M. Brandon, K.D. Cannon, M.J. Koren, D. S. Denham, M. Berhe, D. Fitz-Patrick, L.L. Hammitt, N.P. Klein, H. Nell, G. Keep, X. Wang, K. Koury, K.A. Swanson, D. Cooper, C. Lu, Ö. Türeci, E. Lagkadinou, D. B. Tresnan, P.R. Dormitzer, U. Şahin, W.C. Gruber, K.U. Jansen, C.C.T. Group, Safety and efficacy of a third dose of BNT162b2 covid-19 vaccine, N. Engl. J. Med. 386 (2022) 1910–1921, https://doi.org/10.1056/nejmoa2200674.

[6] R.A. Feldman, R. Fuhr, I. Smolenov, A.(Mick, Ribeiro, L. Panther, M. Watson, J. J. Senn, M. Smith, Örn Almarsson, H.S. Pujar, M.E. Laska, J. Thompson, T. Zaks, G. Ciaramella, mRNA vaccines against H10N8 and H7N9 influenza viruses of pandemic potential are immunogenic and well tolerated in healthy adults in phase 1 randomized clinical trials, Vaccine 37 (2019) 3326–3334, https://doi.org/10.1016/j.vaccine.2019.04.074.

[7] S. Chivukula, T. Plitnik, T. Tibbitts, S. Karve, A. Dias, D. Zhang, R. Goldman, H. Gopani, A. Khanmohammed, A. Sarode, D. Cooper, H. Yoon, Y. Kim, Y. Yan, S. T. Mundle, R. Groppo, A. Beauvais, J. Zhang, N.G. Anosova, C. Lai, L. Li, G. Ulinski, P. Piepenhagen, J. DiNapoli, K.V. Kalnin, V. Landolfi, R. Swearingen, T.-M. Fu, F. DeRosa, D. Casimiro, Development of multivalent mRNA vaccine candidates for seasonal or pandemic influenza, Npj Vaccines 6 (2021) 153, https://doi.org/10.1038/s41541-021-00420-6.

[8] C. Wang, Y. Zhang, Y. Dong, Lipid nanoparticle–mRNA formulations for therapeutic applications, Accounts Chem. Res. 54 (2021) 4283–4293, https://doi.org/10.1021/acs.accounts.1c00550.

[9] M.L. Guevara, F. Persano, S. Persano, Advances in lipid nanoparticles for mRNA-based cancer immunotherapy, Front. Chem. 8 (2020), 589959, https://doi.org/10.3389/fchem.2020.589959.

[10] P.S. Kowalski, A. Rudra, L. Miao, D.G. Anderson, Delivering the messenger: advances in technologies for therapeutic mRNA delivery, Mol. Ther. 27 (2019) 710–728, https://doi.org/10.1016/j.ymthe.2019.02.012.

[11] K.A. Hajj, K.A. Whitehead, Tools for translation: non-viral materials for therapeutic mRNA delivery, Nat. Rev. Mater. 2 (2017), 17056, https://doi.org/10.1038/natrevmats.2017.56.
[12] S. Sabnis, E.S. Kumarasinghe, T. Salerno, C. Mihai, T. Ketova, J.J. Senn, A. Lynn, A. Bulychev, I. McFadyen, J. Chan, Ö. Almarsson, M.G. Stanton, K.E. Benenato, A novel amino lipid series for mRNA delivery: improved endosomal escape and sustained pharmacology and safety in non-human primates, Mol. Ther. 26 (2018) 1509–1519, https://doi.org/10.1016/j.ymthe.2018.03.010.
[13] A. Ahmad, J.M. Khan, S. Haque, Strategies in the design of endosomolytic agents for facilitating endosomal escape in nanoparticles, Biochimie 160 (2019) 61–75, https://doi.org/10.1016/j.biochi.2019.02.012.
[14] M. Maugeri, M. Nawaz, A. Papadimitriou, A. Angerfors, A. Camponeschi, M. Na, M. Hölttä, P. Skantze, S. Johansson, M. Sundqvist, J. Lindquist, T. Kjellman, I.-L. Mårtensson, T. Jin, P. Sunnerhagen, S. Östman, L. Lindfors, H. Valadi, Linkage between endosomal escape of LNP-mRNA and loading into EVs for transport to other cells, Nat. Commun. 10 (2019) 4333, https://doi.org/10.1038/s41467-019-12275-6.
[15] H. Ni, M.Z.C. Hatit, K. Zhao, D. Loughrey, M.P. Lokugamage, H.E. Peck, A.D. Cid, A. Muralidharan, Y. Kim, P.J. Santangelo, J.E. Dahlman, Piperazine-derived lipid nanoparticles deliver mRNA to immune cells in vivo, Nat. Commun. 13 (2022) 4766, https://doi.org/10.1038/s41467-022-32281-5.
[16] K.A. Whitehead, J.R. Dorkin, A.J. Vegas, P.H. Chang, O. Veiseh, J. Matthews, O. S. Fenton, Y. Zhang, K.T. Olejnik, V. Yesilyurt, D. Chen, S. Barros, B. Klebanov, T. Novobrantseva, R. Langer, D.G. Anderson, Degradable lipid nanoparticles with predictable in vivo siRNA delivery activity, Nat. Commun. 5 (2014) 4277, https://doi.org/10.1038/ncomms5277.
[17] O.S. Fenton, K.J. Kauffman, R.L. McClellan, J.C. Kaczmarek, M.D. Zeng, J. L. Andresen, L.H. Rhym, M.W. Heartlein, F. DeRosa, D.G. Anderson, Customizable lipid nanoparticle materials for the delivery of siRNAs and mRNAs, Angew. Chem. Int. Ed. 57 (2018) 13582–13586, https://doi.org/10.1002/anie.201809056.
[18] Y. Eygeris, M. Gupta, J. Kim, G. Sahay, Chemistry of lipid nanoparticles for RNA delivery, Accounts Chem. Res. 55 (2022) 2–12, https://doi.org/10.1021/acs.accounts.1c00544.
[19] M. Kim, M. Jeong, S. Hur, Y. Cho, J. Park, H. Jung, Y. Seo, H.A. Woo, K.T. Nam, K. Lee, H. Lee, Engineered ionizable lipid nanoparticles for targeted delivery of RNA therapeutics into different types of cells in the liver, Sci. Adv. 7 (2021), eabf4398, https://doi.org/10.1126/sciadv.abf4398.
[20] S. Liu, Q. Cheng, T. Wei, X. Yu, L.T. Johnson, L. Farbiak, D.J. Siegwart, Membrane-destabilizing ionizable phospholipids for organ-selective mRNA delivery and CRISPR–Cas gene editing, Nat. Mater. 20 (2021) 701–710, https://doi.org/10.1038/s41563-020-00886-0.
[21] L. Miao, L. Li, Y. Huang, D. Delcassian, J. Chahal, J. Han, Y. Shi, K. Sadtler, W. Gao, J. Lin, J.C. Doloff, R. Langer, D.G. Anderson, Delivery of mRNA vaccines with heterocyclic lipids increases anti-tumor efficacy by STING-mediated immune cell activation, Nat. Biotechnol. 37 (2019) 1174–1185, https://doi.org/10.1038/s41587-019-0247-3.
[22] K.T. Love, K.P. Mahon, C.G. Levins, K.A. Whitehead, W. Querbes, J.R. Dorkin, J. Qin, W. Cantley, L.L. Qin, T. Racie, M. Frank-Kamenetsky, K.N. Yip, R. Alvarez, D.W.Y. Sah, A. de Fougerolles, K. Fitzgerald, V. Koteliansky, A. Akinc, R. Langer, D. G. Anderson, Lipid-like materials for low-dose, in vivo gene silencing, Proc. Natl. Acad. Sci. USA 107 (2010) 1864–1869, https://doi.org/10.1073/pnas.0910603106.
[23] M. Schlich, R. Palomba, G. Costabile, S. Mizrahy, M. Pannuzzo, D. Peer, P. Decuzzi, Cytosolic delivery of nucleic acids: the case of ionizable lipid nanoparticles, Bioeng Transl Medicine 6 (2021), e10213, https://doi.org/10.1002/btm2.10213.
[24] Y. Suzuki, K. Hyodo, T. Suzuki, Y. Tanaka, H. Kikuchi, H. Ishihara, Biodegradable lipid nanoparticles induce a prolonged RNA interference-mediated protein knockdown and show rapid hepatic clearance in mice and nonhuman primates, Int. J. Pharm. 519 (2017) 34–43, https://doi.org/10.1016/j.ijpharm.2017.01.016.
[25] Y. Suzuki, H. Ishihara, Difference in the lipid nanoparticle technology employed in three approved siRNA (Patisiran) and mRNA (COVID-19 vaccine) drugs, Drug Metabol. Pharmacokinet. 41 (2021), 100424, https://doi.org/10.1016/j.dmpk.2021.100424.
[26] M. Jayaraman, S.M. Ansell, B.L. Mui, Y.K. Tam, J. Chen, X. Du, D. Butler, L. Eltepu, S. Matsuda, J.K. Narayanannair, K.G. Rajeev, I.M. Hafez, A. Akinc, M.A. Maier, M. A. Tracy, P.R. Cullis, T.D. Madden, M. Manoharan, M.J. Hope, Maximizing the potency of siRNA lipid nanoparticles for hepatic gene silencing in vivo, Angew. Chem. Int. Ed. 51 (2012) 8529–8533, https://doi.org/10.1002/anie.201203263.
[27] S.M. Ansell, X. Du, WO2015199952A1.pdf, 2015.
[28] K.J. Hassett, K.E. Benenato, E. Jacquinet, A. Lee, A. Woods, O. Yuzhakov, S. Himansu, J. Deterling, B.M. Geilich, T. Ketova, C. Mihai, A. Lynn, I. McFadyen, M.J. Moore, J.J. Senn, M.G. Stanton, Ö. Almarsson, G. Ciaramella, L.A. Brito, Optimization of lipid nanoparticles for intramuscular administration of mRNA vaccines, Mol. Ther. Nucleic Acids 15 (2019) 1–11, https://doi.org/10.1016/j.omtn.2019.01.013.
[29] O.S. Fenton, K.J. Kauffman, R.L. McClellan, E.A. Appel, J.R. Dorkin, M.W. Tibbitt, M.W. Heartlein, F. DeRosa, R. Langer, D.G. Anderson, Bioinspired alkenyl amino alcohol ionizable lipid materials for highly potent in vivo mRNA delivery, Adv. Mater. 28 (2016) 2939–2943, https://doi.org/10.1002/adma.201505822.
[30] Y. Dong, K.T. Love, J.R. Dorkin, S. Sirirungruang, Y. Zhang, D. Chen, R.L. Bogorad, H. Yin, Y. Chen, A.J. Vegas, C.A. Alabi, G. Sahay, K.T. Olejnik, W. Wang, A. Schroeder, A.K.R. Lytton-Jean, D.J. Siegwart, A. Akinc, C. Barnes, S.A. Barros, M. Carioto, K. Fitzgerald, J. Hettinger, V. Kumar, T.I. Novobrantseva, J. Qin, W. Querbes, V. Koteliansky, R. Langer, D.G. Anderson, Lipopeptide nanoparticles for potent and selective siRNA delivery in rodents and nonhuman primates, Proc. Natl. Acad. Sci. USA 111 (2014) 3955–3960, https://doi.org/10.1073/pnas.1322937111.
[31] P. Patel, N.M. Ibrahim, K. Cheng, The importance of apparent pKa in the development of nanoparticles encapsulating siRNA and mRNA, Trends Pharmacol. Sci. 42 (2021) 448–460, https://doi.org/10.1016/j.tips.2021.03.002.
[32] M. Qiu, Y. Li, H. Bloomer, Q. Xu, Developing biodegradable lipid nanoparticles for intracellular mRNA delivery and genome editing, Accounts Chem. Res. 54 (2021) 4001–4011, https://doi.org/10.1021/acs.accounts.1c00500.
[33] C.A. Alabi, K.T. Love, G. Sahay, H. Yin, K.M. Luly, R. Langer, D.G. Anderson, Multiparametric approach for the evaluation of lipid nanoparticles for siRNA delivery, Proc. Natl. Acad. Sci. USA 110 (2013) 12881–12886, https://doi.org/10.1073/pnas.1306529110.
[34] N.E. Good, G.D. Winget, W. Winter, T.N. Connolly, S. Izawa, R.M. Singh, Hydrogen ion buffers for biological research, Biochemistry (Moscow, Russ. Fed.) 5 (1966) 467–477.
[35] F. DeRosa, L. Smith, Y. Shen, Y. Huang, J. Pan, H. Xie, B. Yahalom, M.W. Heartlein, Improved efficacy in a fabry disease model using a systemic mRNA liver depot system as compared to enzyme replacement therapy, Mol. Ther. 27 (2019) 878–889, https://doi.org/10.1016/j.ymthe.2019.03.001.
[36] J. Zhang, H. Fan, D.A. Levorse, L.S. Crocker, Ionization behavior of amino lipids for siRNA delivery: determination of ionization constants, SAR, and the impact of lipid pK a on cationic Lipid−Biomembrane interactions, Langmuir 27 (2011) 1907–1914, https://doi.org/10.1021/la104590k.
[37] K. Koitabashi, H. Nagumo, M. Nakao, T. Machida, K. Yoshida, K. Sakai-Kato, Acidic pH-induced changes in lipid nanoparticle membrane packing, Biochimica Et Biophysica Acta Bba - Biomembr. 1863 (2021), 183627, https://doi.org/10.1016/j.bbamem.2021.183627.
[38] T. Parasassi, G.D. Stasio, G. Ravagnan, R.M. Rusch, E. Gratton, Quantitation of lipid phases in phospholipid vesicles by the generalized polarization of Laurdan fluorescence, Biophys. J. 60 (1991) 179–189, https://doi.org/10.1016/s0006-3495(91)82041-0.
[39] D.N. Mastronarde, Advanced data acquisition from electron microscopes with SerialEM, Microsc. Microanal. 24 (2018) 864–865, https://doi.org/10.1017/s1431927618004816.
[40] K.V. Kalnin, T. Plitnik, M. Kishko, D. Huang, A. Raillard, J. Piolat, N.G. Anosova, T. Tibbitts, J. DiNapoli, S. Karve, R. Goldman, H. Gopani, A. Dias, K. Tran, M. Zacharia, X. Gu, L. Boeglin, J. Abysalh, J. Vargas, A. Beaulieu, M. Shah, T. Jeannotte, K. Gillis, S. Chivukula, R. Swearingen, V. Landolfi, T.-M. Fu, F. DeRosa, D. Casimiro, Pan-SARS neutralizing responses after third boost vaccination in non-human primate immunogenicity model, Vaccine 40 (2022) 1289–1298, https://doi.org/10.1016/j.vaccine.2022.01.021.
[41] G.J. Pielak, Buffers, especially the Good kind, Biochemistry-Us 60 (2021) 3436–3440, https://doi.org/10.1021/acs.biochem.1c00200.
[42] K.J. Kauffman, F.F. Mir, S. Jhunjhunwala, J.C. Kaczmarek, J.E. Hurtado, J.H. Yang, M.J. Webber, P.S. Kowalski, M.W. Heartlein, F. DeRosa, D.G. Anderson, Efficacy and Immunogenicity of Unmodified and Pseudouridine- Modified mRNA Delivered Systemically with Lipid Nanoparticles in Vivo, Biomaterials, 2016, pp. 78–87.
[43] R.S. Riley, M.V. Kashyap, M.M. Billingsley, B. White, M.-G. Alameh, S.K. Bose, P. W. Zoltick, H. Li, R. Zhang, A.Y. Cheng, D. Weissman, W.H. Peranteau, M. J. Mitchell, Ionizable lipid nanoparticles for in utero mRNA delivery, Sci. Adv. 7 (2021).
[44] A. Wahane, A. Waghmode, A. Kapphahn, K. Dhuri, A. Gupta, R. Bahal, Role of lipid-based and polymer-based non-viral vectors in nucleic acid delivery for next-generation gene therapy, Molecules 25 (2020) 2866, https://doi.org/10.3390/molecules25122866.
[45] M. Amaro, F. Reina, M. Hof, C. Eggeling, E. Sezgin, Laurdan and Di-4-ANEPPDHQ probe different properties of the membrane, J. Phys. D Appl. Phys. 50 (2017), 134004, https://doi.org/10.1088/1361-6463/aa5dbc.
[46] R. Šachl, M. Štěpánek, K. Procházka, J. Humpolícková, M. Hof, Fluorescence study of the solvation of fluorescent probes prodan and laurdan in poly(ε-caprolactone)-block-poly(ethylene oxide) vesicles in aqueous solutions with tetrahydrofurane, Langmuir 24 (2008) 288–295, https://doi.org/10.1021/la702277t.
[47] K.J. Hassett, J. Higgins, A. Woods, B. Levy, Y. Xia, C.J. Hsiao, E. Acosta, Ö. Almarsson, M.J. Moore, L.A. Brito, Impact of lipid nanoparticle size on mRNA vaccine immunogenicity, J. Contr. Release 335 (2021) 237–246, https://doi.org/10.1016/j.jconrel.2021.05.021.
[48] P.P.G. Guimaraes, R. Zhang, R. Spektor, M. Tan, A. Chung, M.M. Billingsley, R. El-Mayta, R.S. Riley, L. Wang, J.M. Wilson, M.J. Mitchell, Ionizable lipid nanoparticles encapsulating barcoded mRNA for accelerated in vivo delivery screening, J. Contr. Release (2019) 404–417. https://reader.elsevier.com/reader/sd/pii/S0168365919305929?token=DD933081D67E4A925DAA032205932CD08828C0AD7574C1F9445413D237C61A6EECE6DC72502400243CB074FD96139CAF&;originRegion=us-east-1&originCreation=20220822192118.
[49] L. Schoenmaker, D. Witzigmann, J.A. Kulkarni, R. Verbeke, G. Kersten, W. Jiskoot, D. Crommelin, mRNA-lipid nanoparticle COVID-19 vaccines: structure and stability, Int. J. Pharm. 601 (2021), 120586, https://doi.org/10.1016/j.ijpharm.2021.120586.
[50] M.L. Brader, S.J. Williams, J.M. Banks, W.H. Hui, Z.H. Zhou, L. Jin, Encapsulation state of messenger RNA inside lipid nanoparticles, Biophys. J. 120 (2021) 2766–2770, https://doi.org/10.1016/j.bpj.2021.03.012.
[51] M. Kloczewiak, J.M. Banks, L. Jin, M.L. Brader, A biopharmaceutical perspective on higher-order structure and thermal stability of mRNA vaccines, Mol. Pharm. 19 (2022) 2022–2031, https://doi.org/10.1021/acs.molpharmaceut.2c00092.
[52] A.K.K. Leung, Y.Y.C. Tam, S. Chen, I.M. Hafez, P.R. Cullis, Microfluidic mixing: a general method for encapsulating macromolecules in lipid nanoparticle systems,

J. Phys. Chem. B 119 (2015) 8698–8706, https://doi.org/10.1021/acs.jpcb.5b02891.
[53] M.Y. Arteta, T. Kjellman, S. Bartesaghi, S. Wallin, X. Wu, A.J. Kvist, A. Dabkowska, N. Székely, A. Radulescu, J. Bergenholtz, L. Lindfors, Successful reprogramming of cellular protein production through mRNA delivered by functionalized lipid nanoparticles, Proc. Natl. Acad. Sci. USA 115 (2018) E3351–E3360, https://doi.org/10.1073/pnas.1720542115.
[54] Y. Eygeris, S. Patel, A. Jozic, G. Sahay, Deconvoluting lipid nanoparticle structure for messenger RNA delivery, Nano Lett. 20 (2020) 4543–4549, https://doi.org/10.1021/acs.nanolett.0c01386.
[55] K. Bahl, J.J. Senn, O. Yuzhakov, A. Bulychev, L.A. Brito, K.J. Hassett, M.E. Laska, M. Smith, Ö. Almarsson, J. Thompson, A.(Mick, Ribeiro, M. Watson, T. Zaks, G. Ciaramella, Preclinical and clinical demonstration of immunogenicity by mRNA vaccines against H10N8 and H7N9 influenza viruses, Mol. Ther. 25 (2017) 1316–1327, https://doi.org/10.1016/j.ymthe.2017.03.035.
[56] A.B. Vogel, L. Lambert, E. Kinnear, D. Busse, S. Erbar, K.C. Reuter, L. Wicke, M. Perkovic, T. Beissert, H. Haas, S.T. Reece, U. Sahin, J.S. Tregoning, Self-amplifying RNA vaccines give equivalent protection against influenza to mRNA vaccines but at much lower doses, Mol. Ther. 26 (2018) 446–455, https://doi.org/10.1016/j.ymthe.2017.11.017.